Biosensors and Bioelectronics 168 (2020) 112571

Contents lists available at ScienceDirect

Biosensors and Bioelectronics

journal homepage: http://www.elsevier.com/locate/bios

High-performance FRET biosensors for single-cell and *in vivo* lead detection

De-Ming Yang [a,b,c,*], Tsai-Feng Fu [d,1], Choun-Sea Lin [e,1], Tai-Yu Chiu [a,1], Chien-Chang Huang [f], Hsin-Yi Huang [a,g], Min-Wen Chung [g], Yu-Syuan Lin [a], Robeth Viktoria Manurung [h], Phan Nguyen Nhi Nguyen [g], Yu-Fen Chang [g,**]

[a] *Microscopy Service Laboratory, Basic Research Division, Department of Medical Research, Taipei Veterans General Hospital, Taipei, 11217, Taiwan*
[b] *Institute of Biophotonics, National Yang-Ming University, 155 Sec-2, Li Nong Street, Taipei, 11221, Taiwan*
[c] *Biophotonics and Molecular Imaging Research Center (BMIRC), National Yang-Ming University, Taipei, 11221, Taiwan*
[d] *Department of Applied Chemistry, National Chi-Nan University, Nantou, 54561, Taiwan*
[e] *Agricultural Biotechnology Research Center (ABRC), Academia Sinica, Taipei, 115, Taiwan*
[f] *Core Facilities for Translational Medicines, BioTReC, Academia Sinica, Taipei, 115, Taiwan*
[g] *LumiSTAR Biotechnology, Inc., National Biotechnology Research Park, Taipei, 115, Taiwan*
[h] *Research Center for Electronics and Telecommunication, Indonesian Institute of Sciences (LIPI), Indonesia*

ARTICLE INFO

Keywords:
Intracellular Pb^{2+} contents
Pb^{2+} biosensor
FRET
In vivo biosensing
Drosophila
Arabidopsis

ABSTRACT

Forms of lead (Pb) have been insidiously invading human life for thousands of years without obvious signs of their considerable danger to human health. Blood lead level (BLL) is the routine measure used for diagnosing the degree of lead intoxication, although it is unclear whether there is any safe range of BLL. To develop a practical detection tool for living organisms, we engineered a genetically encoded fluorescence resonance energy transfer (FRET)-based Pb^{2+} biosensor, 'Met-lead 1.44 M1', with excellent performance. Met-lead 1.44 M1 has an apparent dissociation constant (K_d) of 25.97 nM, a detection limit (LOD) of 10 nM (2.0 ppb/0.2 μg/dL), and an enhancement dynamic ratio of nearly ~ 5-fold upon Pb^{2+} binding. The 10 nM sensitivity of Met-lead 1.44 M1 is five times below the World Health Organization-permitted level of lead in tap water (10 ppb; WHO, 2017), and fifteen times lower than the maximum BLL for children (3 μg/dL). We deployed Met-lead 1.44 M1 to measure Pb^{2+} concentrations in different living models, including two general human cell lines and one specific line, induced pluripotent stem cell (iPSC)-derived cardiomyocytes, as well as in widely used model species in plant (*Arabidopsis thaliana*) and animal (*Drosophila melanogaster*) research. Our results suggest that this new biosensor is suitable for lead toxicological research *in vitro* and *in vivo*, and will pave the way toward potential applications for both low BLL measures and rapid detection of environmental lead in its divalent form.

1. Introduction

Various forms of the heavy metal lead (Pb) are abundant in our environment, e.g. air, water, and soil, and even within living organisms (Frank et al., 2019). For the past 3000 years, lead has been used for purposes ranging from wine adulteration, paints, gasoline and hair dyes to water pipes (O'Connor et al., 2020). Lead has quietly invaded human life without revealing obvious signs of its considerable health dangers (Needleman, 2004; Flora et al., 2012). In fact, the dark side of this metal might never have been discovered but for the efforts of the American geochemist Clair C. Patterson (1965), who determined the age of the Earth through examination of the isotopic composition of lead (Patterson, 1956). He later noticed an association between human health problems and lead levels, primarily derived from leaded gasoline. Statistical analysis of a 20-year data set suggested that over 400,000 people die in the U.S. per year due to lead exposure. Lead inside the human body is a risk factor that contributes to both cardiovascular disease and overall mortality rate (Lanphear et al., 2018). In addition, numerous children may suffer possibly permanent cognitive damage or neurodegenerative diseases due to lead exposure (Reuben et al., 2017).

* Corresponding author. Microscopy Service Laboratory, Basic Research Division, Department of Medical Research, Taipei Veterans General Hospital, Taipei, 11217, Taiwan.
** Corresponding author.
E-mail addresses: dmyang@vghtpe.gov.tw (D.-M. Yang), yu-fen.chang@lumistar.com.tw (Y.-F. Chang).
[1] Equal contribution to this study.

https://doi.org/10.1016/j.bios.2020.112571
Received 1 June 2020; Received in revised form 25 August 2020; Accepted 27 August 2020
Available online 31 August 2020

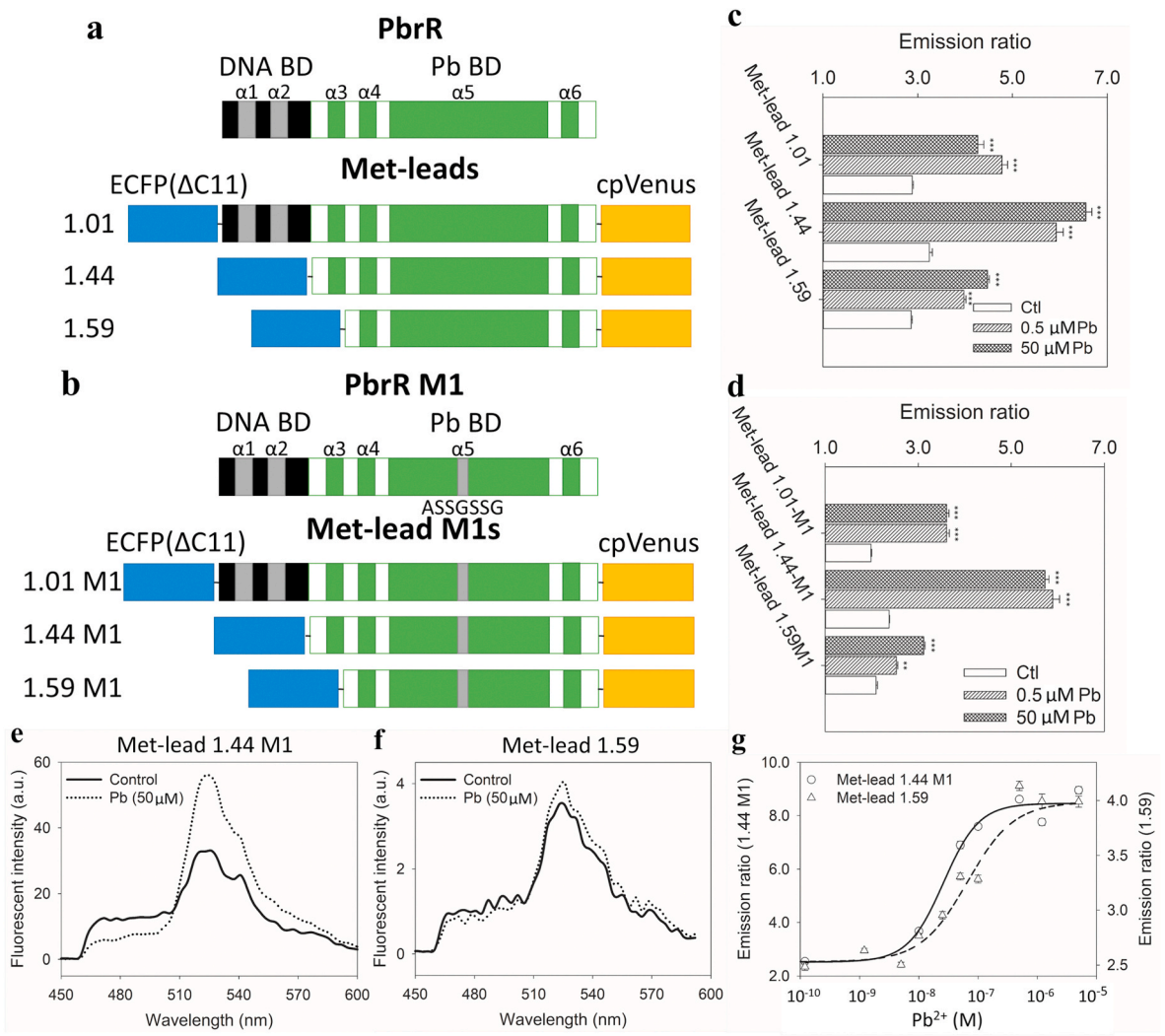

Fig. 1. Met-leads FRET sensors designed for Pb^{2+} detection. (a) Protein domains of PbrR and the designed Met-leads. PbrR contains a DNA binding domain (BD) and a Pb BD. The six α-helices of PbrR, numbered 1–6, are shown in gray (α1 and α2) and green (α3–α6). All Met-lead versions have the same FRET pairs, ECFP(ΔC11) (blue) and cpVenus (yellow). (b) Protein domains of the M1 Met-lead versions, showing the linker, ASSGSSG, inserted in PbrR α-helix 5. (c, d) Emission ratios (cpVenus/ECFP(ΔC11)) of Met-leads 1.01, 1.44, and 1.59 (c) and the corresponding M1 versions (d) with or without Pb^{2+}. (e, f) In-cell fluorescence emission spectra of Met-leads without (solid line) or with (dotted line) 50 μM Pb^{2+}. (g) In-cell titration data for Met-leads (circles, 1.44 M1; triangles, 1.59) at different Pb^{2+} concentrations. (For interpretation of the references to color in this figure legend, the reader is referred to the Web version of this article.)

It was recently suggested that the blood lead level (BLL), the amount of lead in the blood, should not exceed 3.5–5 μg/dL (~175–250 nM) in adults and less than 3 μg/dL (150 nM) in children (Lanphear et al., 2018). Over time, scientists have gathered increasing evidence that no minimal BLL is actually safe, if safety is defined as a total absence of harm (Reuben et al., 2017; Lanphear et al., 2018; Rocha and Trujillo, 2019). For example, children subjected to long-term exposure to even very low BLLs still have a high probability of developing neurodevelopmental impairments, including scoring lower on intelligence quotient (IQ) tests, exhibiting academic deficits and suffering from attention deficit hyperactivity disorder (ADHD), although the development of these disorders may not be associated with clear obvious symptoms or specific behavior alterations (Reuben et al., 2017; Rocha and Trujillo, 2019). To assess the toxicological mechanisms behind lead exposure, it would be extremely valuable for human health to develop an effective method to precisely measure very low amounts of lead (e.g. <150 nM) inside living organisms and determine accumulation routes (Caldwell et al., 2017, 2019; Paulson and Brown, 2019).

Over the years, through countless efforts to modify and combine them, fluorescent protein (FP)-based biosensors, also known as genetically encoded indicators, have become widely used in many fields. FP biosensors were first developed to measure intracellular calcium, based on the detection of fluorescence resonance energy transfer (FRET) events between two FPs (Miyawaki et al., 1997). Inspired by this classic "cameleon" sensor, various FRET-based biosensors have been developed to specifically display the detailed status of living cells dynamically and/or to precisely predict the fate of targeted cells (Azad et al., 2014; Carter et al., 2014; Hochreiter et al., 2015; Bischof et al., 2019; Hosseini et al., 2020). To study lead poisoning, we previously developed the first FRET-based lead biosensor Met-lead 1.59 to detect the inorganic divalent form of lead (Pb^{2+}), with a dynamic range (DR, in fold of FRET-ratio value) of 172% (from 3.3 to 5.7 at 50 μM) and a sensitivity (limit of detection, LOD) after a 3-h exposure to 500 nM lead, just below the now disused adult BLL threshold of 10 μg/dL (Chiu and Yang, 2012). To further improve the visualization of lead intoxication *in vivo*, we developed a new series of Pb^{2+} biosensors, the Met-leads, with different sensing abilities. The DR of the best version, Met-lead 1.44 M1, rose to 460% (at 10 μM), while its LOD dropped to 10 nM (0.2 μg/dL or 2.0 ppb), which is five times lower than the World Health Organization (WHO)-permitted level of Pb^{2+} in tap water (10 ppb; WHO, 2017) and fifteen times lower than the maximum BLL for children, 3 μg/dL. We also tested this biosensor in a variety of hosts, from single living human cells

to plant cotyledons and Drosophila organs to whole flies, to assess its sensing capability via in-cell, *ex vivo* and *in vivo* modalities.

2. Materials and methods

2.1. Gene construction

To construct a FRET-based lead biosensor, we previously tested different lead binding proteins, isolated from the lead resistance operon (*Pbr*) of the bacterium *Cupriavidus metallidurans* CH34, e.g. PbrA, PbrD, and PbrR (Borremans et al., 2001), as candidates for a lead sensing domain within the FRET biosensor design. Only PbrR performed well in the generation of FRET events upon binding of lead ions (Chiu and Yang, 2012). We PCR-amplified the *PbrR* gene fragment and cloned the PCR product into the pGEM-T easy vector (Promega). We inserted the 7-residue ASSGSSG linker (Fig. 1b) between amino acids 98 and 99 of PbrR, thereby breaking one α-helix critical for dimerization into two short α-helixes to allow for some flexibility (Figs. S5 and S6). We then PCR-amplified the full-length (aa 1–131) and two truncated forms (aa 44–131 and aa 59–131) of PbrR with or without the ASSGSSG linker using primers containing the *Kpn*I and *Bam*HI restriction sites. We then substituted the resulting *Kpn*I/*Bam*HI fragments for the region in Met-lead/pcDNA3 coding for the Pb^{2+}-binding domain (PbBD), to generate Met-lead 1.01, 1.44, 1.59, and 1.01 M1, 1.44 M1, 1.59 M1, respectively (Fig. S1).

2.2. Molecular structure and simulation of met-leads

We predicted the molecular structures of Met-leads and related proteins in this study, i.e. the cyan fluorescent protein (CFP), the circular permutated yellow fluorescent protein (YFP) variant cpVenus, and the Met-lead biosensor series (containing the above FRET pairs and the PbrR sensing peptides) through the homology modeling-based prediction server PS2 (Chen et al., 2006; Huang et al., 2015; Yang et al., 2020). In the Molecular Operating Environment software (MOE, Chemical Computing Group Inc., with the help of Professor Wolfgang Fischer, Institute of Biophotonics, National Yang-Ming University) (MOE, 2013), we analyzed the sequence of proteins of interests, including join chain and energy calculation, and exported the data as a. mol2 file. We then used Pymol to generate animated display files (Movies S1, S2).

Supplementary data related to this article can be found at https://doi.org/10.1016/j.bios.2020.112571.

2.3. Human cell cultures, gene transfer, and procedure for FRET imaging

We introduced the Met-lead biosensors into single human living cells from different sources to examine its sensing abilities. We obtained human embryonic kidney (HEK 293) cells and the human cancer cell line HeLa from the American Type Culture Collection (ATCC, Rockville, MD). Cell lines were cultured according to the culture manual (Chiu and Yang, 2012; Chiu et al., 2013). Human induced pluripotent stem cells (iPSC)-derived cardiomyocytes (Cardiosight®-S) (Wang et al., 2015; Uzun et al., 2016) were obtained from Nexel (Seoul, South Korea). We first coated 96-well glass-bottom plates with fibronectin/gelatin (0.5%/0.1%) at 37 °C for at least 1 h. We then plated human iPSC cardiomyocytes in the 96-well glass-bottom plates and cultured them for three days in Nexel's Cardiomyocyte Maintenance Medium, at which point cells were ready for observation with Tyrode's buffer. For further FRET imaging, we seeded human cells on 24 mm coverglasses (Deckglaser) coated with poly-L-lysine and transfected them with the genes encoding Met-leads using LipofectAmine (Invitrogen, Thermo Fisher Scientific Inc.) according to the manual (Chang et al., 2008; Chiu and Yang, 2012; Chiu et al., 2013). The cells were used for lead biosensing 2 days after transfection.

2.4. Cultures of plant protoplasts/seedlings/whole plant, gene transfer, and procedure for FRET imaging

We generated and cultured Arabidopsis (*Arabidopsis thaliana*) protoplasts from Col-0 seedlings according to the culture manual (Wu et al., 2009). We introduced the genes encoding Met-lead variants into protoplasts via polyethylene glycol (PEG)-mediated transfection. The protoplasts were put on 24 mm coverglass slides on an inverted FRET imaging platform.

For cotyledon tissues of Arabidopsis seedlings, we followed the AGROBEST method for Agrobacterium (*Agrobacterium tumefaciens*)-mediated transient expression of our FRET sensors, including the introduction of the vectors containing the Met-lead genes in Agrobacterium (Zhang et al., 2006; Wu et al., 2014). We co-cultivated Arabidopsis seedlings and Agrobacterium cultures carrying the Met-lead constructs for 2 days, then washed the Agrobacteria off and allowed the seedlings to grow for another 2–3 days (Zhang et al., 2006; Wu et al., 2014). We then excised the cotyledons and immersed them into leaded water (or pure water for negative controls) overnight before imaging them in an upright FRET imaging platform for *ex vivo* lead biosensing.

We also generated stable transgenic Arabidopsis lines (in the Col-0 background) expressing various Met-lead biosensors using the floral-dipping method (Zhang et al., 2006). We selected primary transformants on Murashige and Skoog (MS) medium supplemented with hygromycin and timentin for 7–10 days (Zhang et al., 2006). We used whole plants for *in vivo/ex vivo* lead biosensing. After 2 days of growth on normal growth medium, we transferred seedlings to leaded medium and excised leaves and imaged them under a stereo FRET imaging platform.

2.5. Fly strains, fly transgene constructs, and preparation for FRET imaging

Drosophila (*Drosophila melanogaster*) fly stocks were raised on standard cornmeal food and housed at 25 °C and 70% relative humidity in a 12:12 h light:dark cycle incubator. The cholinergic *gal4* driver and the specific mushroom bodies driver *R13F02-gal4* (Hu et al., 2010) were a kind gift from Professor Chia-Lin Wu (CGU, Taiwan). We purchased the pan-neuronal driver *Elav-gal4* (#458) from the Bloomington Drosophila Stock Center (BDSC, University of Indiana, IN, USA). We generated *UAS-Met-lead 1.44 M1* and *UAS-Met-lead 1.59* transgenic fly lines. All brain images of transgenic Met-lead expression were collected on the progeny of crosses between *gal4* driver lines and the *UAS-Met-lead 1.44 M1* or *UAS-Met-lead 1.59* indicator lines.

We generated the pUAST-Met-lead 1.44 M1 and pUAST-Met-lead 1.59 constructs using standard molecular cloning procedures. We first digested the pcDNA3-Met-lead 1.44 M1 or pcDNA3-Met-lead 1.59 vectors with *Hind*III and filled in the cohesive ends to obtain blunt ends. We then digested the linearized vectors with *Xho*I for the release of the 1.7 kbp Met-lead 1.44 M1 or Met-lead 1.59 genes. We then cloned the Met-lead 1.44 M1 and Met-lead 1.59 fragments into the filled-in *Not*I and cohesive *Xho*I site of the double-digested pJFRC28-10XUAS-IVS-GFP-p10 vector (plasmid#36431; purchased from Addgene) to create the pUAST-Met-lead 1.44 M1 and pUAST-Met-lead 1.59 transgenes, respectively. We generated the *UAS-Met-lead 1.44 M1* and *UAS-Met-lead 1.59* flies by injecting the transgenes into embryos, using a standard protocol for phiC31-mediated specific insertion on chromosome II attP40 or on chromosome III attP2 landing sites.

For *in vivo* FRET imaging of the adult brain, we placed flies onto a custom-made plate (Fig. S15A) and removed their skulls on that holder (Fig. S15B) under an upright microscope. For *ex vivo* confocal ratio or spectra imaging, we dissected and immersed adult fly brains in 4% paraformaldehyde (in 0.01 M phosphate-buffered saline, PBS) precooled on ice (30 min before dissection) for 1 h with gentle shaking. The brains were transferred to 2% PBST (PBS with 2% Triton X-100) for 30 min with gentle shaking. We then transferred brain samples to fresh

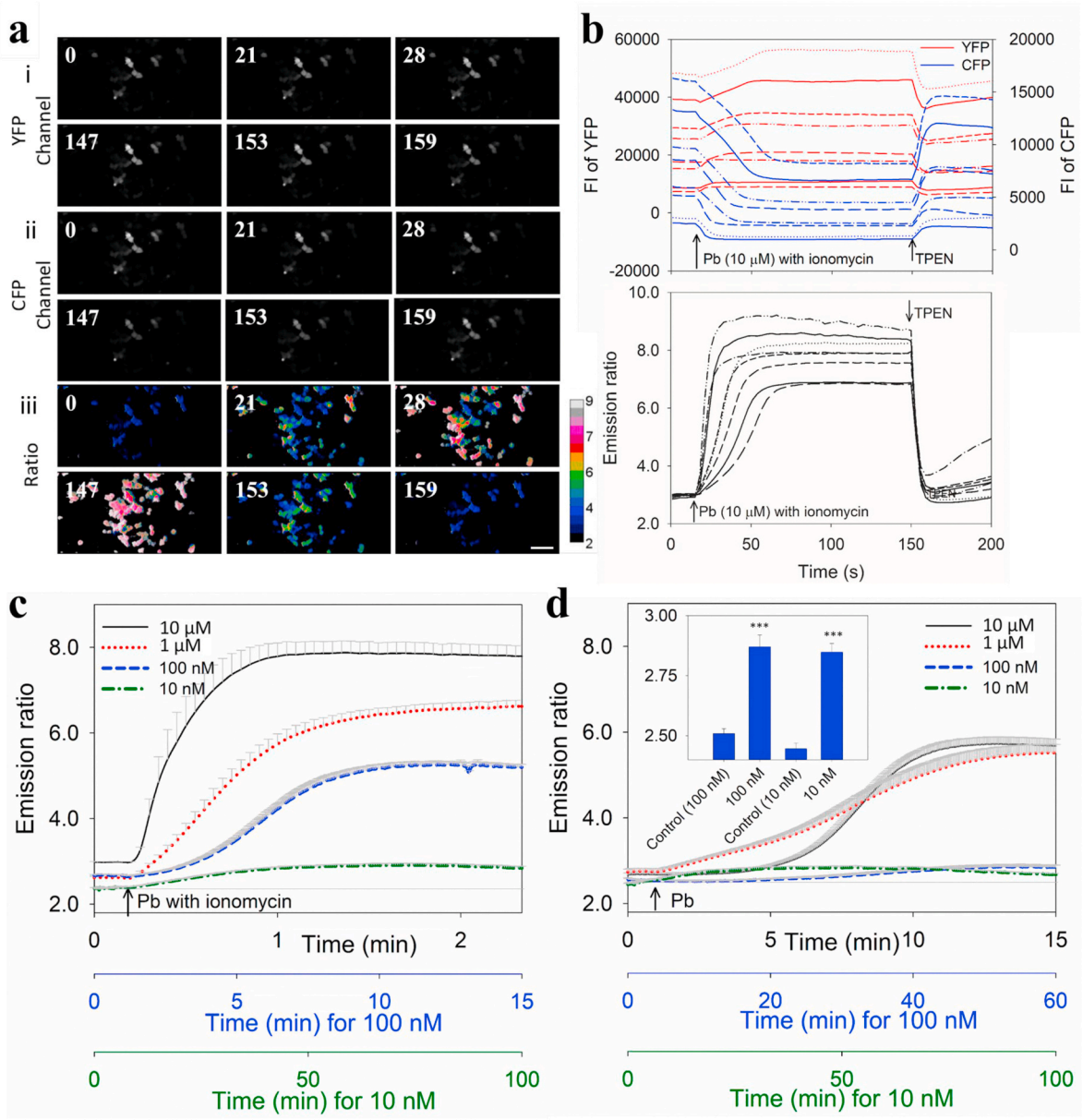

Fig. 2. Live-cell biosensing of intracellular Pb^{2+} by Met-lead 1.44 M1 through an inverted FRET-based image platform. (a) Time-lapse fluorescence images of HeLa cells expressing Met-lead 1.44 M1. Representative images of cpVenus in the YFP channel (i; numbers indicate time points in sec), ECFP(ΔC11) in the CFP channel (ii), and the transformed ratio images as a rainbow color scale (cpVenus/ECFP(ΔC11), iii) are shown. Scale bar, 10 μm; the rainbow-colored ratio bar is from 2 to 9. (b) Representative time courses of FIs for YFP (red) and CFP (blue) channels, and emission ratios from selected cells. 10 μM Pb^{2+}, 5 μM ionomycin and 100 μM TPEN were introduced at the time points indicated by arrows. (c, d) Averaged emission ratios in response to different extracellular Pb^{2+} concentrations (10 μM —, 1 μM ‥, 100 nM ———, 10 nM ‥‥‥) with (c) or without (d) ionomycin. Inset of (d) shows the ratio values at time points before (Control) and after addition of Pb^{2+} at 50 min to 100 nM or 10 nM final. (For interpretation of the references to color in this figure legend, the reader is referred to the Web version of this article.)

2% PBST and placed them in a vacuum chamber to eliminate tracheal air (6 rounds, repeating vacuum 3 min and wait 10 min). We washed the brains three times with PBS with gentle shaking at room temperature, each time for 10 min. Finally, we mounted the sample brains and cleared them with 15 μL of RapiClear on the coverslips. Samples were stored in an electronic dry cabinet until imaging.

2.6. *FRET-ratio imaging or spectra under epi-fluorescent or confocal microscopes*

Met-lead expressing cells (such as HEK 293, HeLa, iPSC-induced cardiomyocytes and protoplasts) or tissues (Arabidopsis cotyledons and Drosophila brains) were imaged on an inverted live-cell (Axiovert 200 M; with 20x objectives, NA = 0.8, Zeiss) or upright *ex vivo/in vivo* (BX-53, Olympus, Japan; with 10x or 20x objectives, NA 0.75 or 0.8, Olympus) FRET-ratio imaging platform, respectively.

To obtain in-cell or *in situ* epi-fluorescent signals of cp173Venus and ECFP(ΔC11) from Met-lead expressing samples, both FRET-ratio image systems (inverted or upright) were equipped with a W-View module (Gemini, Hamamatsu, Japan; with filters 542/27 nm for YFP and 483/32 nm for CFP) and a CMOS camera (ORCA-Flash 4.0 LT, Hamamatsu, Japan) and controlled by HCImage software. For 3D FRET-ratio imaging of fly brains, we employed a laser scanning confocal microscope. We applied a 440 nm laser as the excitation source within either an Olympus FV1000 (with 20x NA 0.75 objectives, Japan) or a Zeiss LSM 880 (with 20x NA 0.8 objectives, Germany) confocal system. We acquired the emission signals, either for YFP (530–630 nm) or CFP (460–500 nm) or a range of emission spectra (from 450 nm to 600 nm) separately or

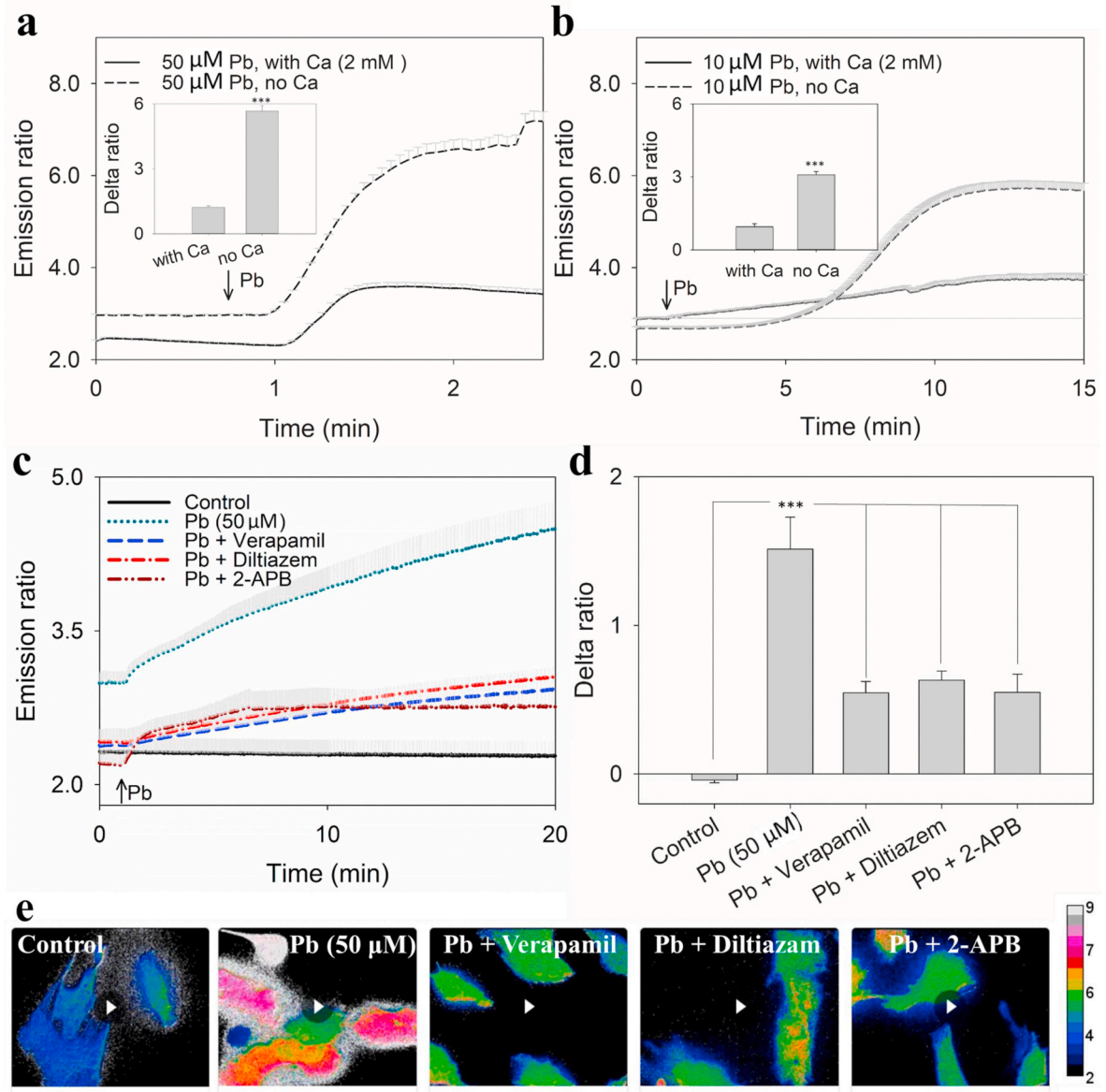

Fig. 3. Pb^{2+} entry through non-selective Ca^{2+} channels. (a, b) Time-lapse recording of HeLa cells expressing Met-lead 1.44 M1 treated with extracellular Pb^{2+} concentrations of 50 μM (a) and 10 μM (b) in the presence (–) or absence (—) of 2 mM extracellular Ca^{2+}. (c, d, e) Time-lapse of Met-lead 1.44 M1 expressed in iPSC-derived cardiomyocytes with 50 μM Pb^{2+} in the presence of the Ca^{2+} channel inhibitors verapamil (————), diltiazam (-.-.-.-.), or 2-APB (-..-..-..-). The Δ ratio (the plateau value of the FRET emission ratio minus the FRET ratio before the introduction of Pb^{2+}) in different conditions are summarized in (a, b, d) as bar graphs. Ratiometric images are shown in e.

continuously.

2.7. FRET-ratio data analysis

We used ImageJ software to calculate the ratio between fluorescent signals for cp173Venus and ECFP(ΔC11) (ratio plus), and to display the ratio as a rainbow color scale to visualize FRET biosensing from blue to red within intact living human cells, plant cotyledons, or fly brains *in vivo*. All experiments were carried out three times with at least three different sets of tested samples (cells, protoplasts, plants, and fly brains). Data gathered from the different batches were integrated to calculate the emission ratio. We tested for statistically significant changes with the two-tailed *t*-test function in the IBM SPSS statistics package, with a *p*-value <0.0005 (***).

3. Results and discussion

3.1. Design and characteristics of lead biosensors

Based on classical FRET strategies (Miyawaki et al., 1997), we designed the Met-leads to comprise two parts: the Pb^{2+}-sensing peptide from PbrR and a pair of FRET FPs, enhanced CFP ECFP(ΔC11) and cp173Venus (Fig. 1a and b; sequences are listed in Fig. S1) (Chiu and Yang, 2012; Yang et al., 2020). We developed six Met-lead versions with Pb-binding domains (BD) of different lengths, and without and with an additional linker, ASSGSSG, designed to prevent multimer formation (Fig. S1): Met-leads 1.01, 1.44, and 1.59 (Met-leads, Fig. 1a) and the corresponding M1 versions with linker (Met-lead M1s, Fig. 1B). We confirmed the success of this M1 linker strategy by gel electrophoresis (Figs. S2 and S3) and homology simulations (Figs. S4–S6). The dimerization properties of PbrR and Met-leads can also be observed through homology simulations (Figs. S7–S9; animated Met-lead 1.44 and

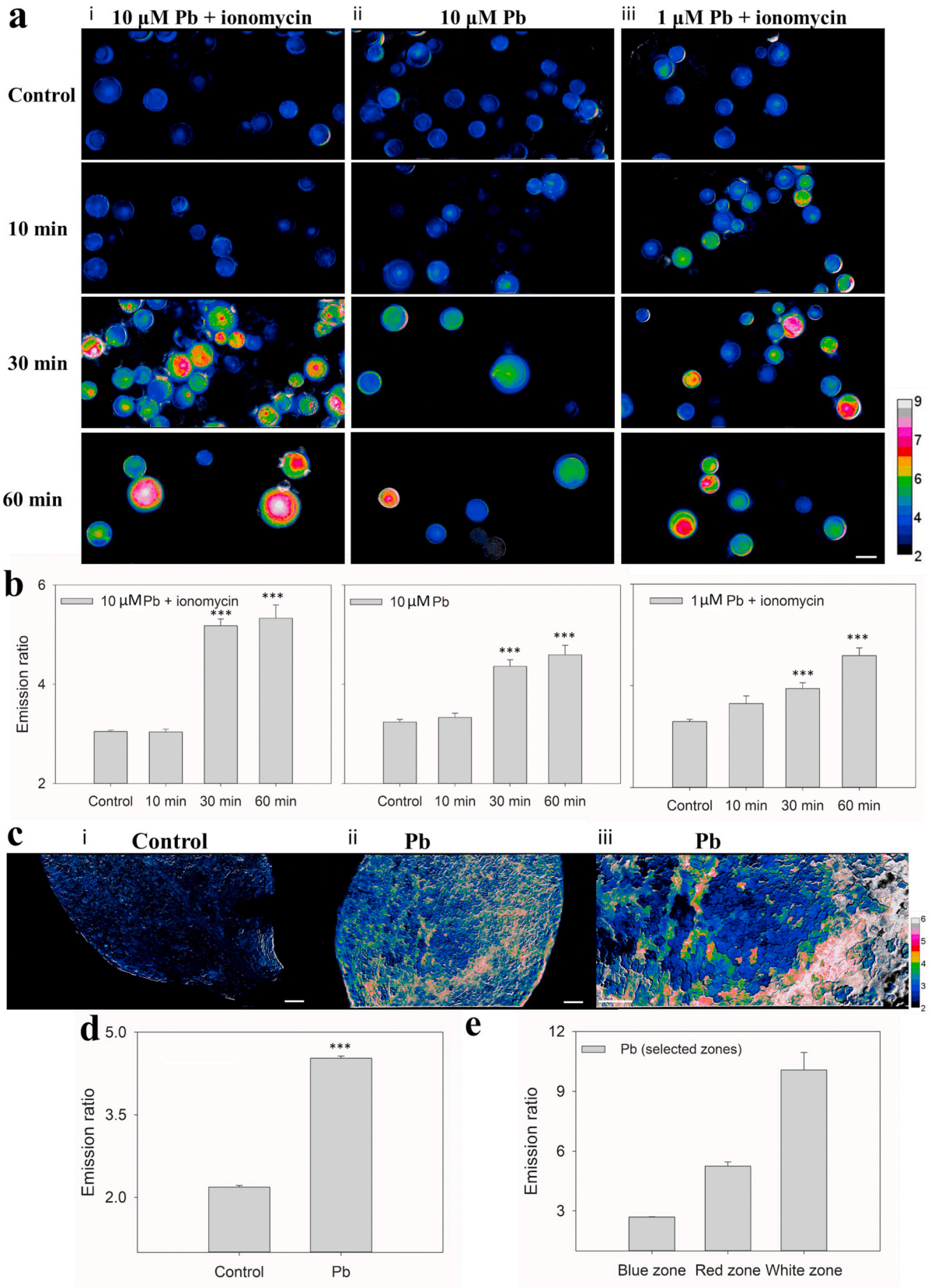

Fig. 4. Detection of intracellular Pb^{2+} using Met-lead 1.44 M1 in Arabidopsis. (a) FRET images acquired at different time points from protoplasts exposed to 10 μM extracellular Pb^{2+} with (i) or without (ii) ionomycin (5 μM), or to 1 μM extracellular Pb^{2+} with ionomycin (iii). (b) Averaged emission ratios of FRET images shown in (a). (c) Acquired FRET images of Arabidopsis cotyledons before (as control; i) and after (ii) they were soaked overnight in 10 μM extracellular Pb^{2+}. (iii) Magnification of the selected region from (ii). (d) Averaged emission ratios of (c., ii). (e) Averaged emission ratios of three selected zones of the image of (c, iii) colored in blue, red, and white (reflecting different intracellular Pb^{2+} concentrations). Scale bars: 10 μm (a), 50 μm (c). (For interpretation of the references to color in this figure legend, the reader is referred to the Web version of this article.)

Met-lead 1.59 are shown in Movie S1 and S2, respectively) and previous reports (Changela et al., 2003; Chen et al., 2005; Sameach et al., 2017).

Next, to validate the FRET design, we expressed all six Met-leads in cultured human cells (HEK 293) that we then exposed to Pb^{2+}. Taking Met-lead 1.44 M1 and 1.59 as examples (Fig. 1e and f), the addition of Pb^{2+} resulted in both an increase in fluorescence of cp173Venus (emission signals obtained from 530 nm to 630 nm) and a decrease in fluorescence from ECFP(ΔC11) (emission signals obtained from 460 nm to 500 nm), confirming that a FRET event occurred, which allowed us to make a ratiometric determination between the two signals (cp173Venus/ECFP(ΔC11)).

In-cell emission ratios of the six Met-leads (Fig. 1c and d) showed that Met-lead 1.44 M1 has a sensing range of ~250% (the ratio increases from 2.37 ± 0.01 to 5.89 ± 0.08, Table S1), which is significantly superior to that of Met-lead 1.59, ~157% (from 2.86 ± 0.02 to 4.48 ± 0.04, Table S2). Results of Pb^{2+} titration experiments in HEK 293 cells expressing Met-lead 1.44 M1 (○) or Met-lead 1.59 (Δ) (Fig. 1g) revealed sensing ranges of at least 350% (from 2.54 ± 0.02 to 8.95 ± 0.14) for Met-lead 1.44 (Table S1) and ~160% (from 2.51 ± 0.02 to 4.03 ± 0.04) for Met-lead 1.59 (Table S2). When we plotted the emission ratios against the Pb^{2+} concentrations and fitted them to a sigmoidal binding function to determine the dissociation constant (K_d), we obtained K_d values of 25.97 nM (~0.5 μg/dL, ~5.0 ppb) and 66.11 nM (1.25 μg/dL) for Met-lead 1.44 M1 and 1.59, respectively. As shown in Fig. 1d and g, the FRET signals of Met-lead 144 M1 were saturated for Pb^{2+} concentrations around or above 0.5 μM (that is, the emission ratio remained the same between 0.5 μM and 50 μM Pb^{2+}), suggesting that this Met-lead version may constitute a good tool to sense Pb^{2+} at relatively low concentrations. The ion selectivity of the optimized Met-lead 1.44 M1 is shown in Figure S10, and is very similar to that of Met-lead 1.59 (Chiu and Yang, 2012).

Because Met-lead 1.44 M1 had the best performance out of our six Met-lead versions in terms of K_d and dynamic range (DR), we deployed it to monitor Pb^{2+} in different living organisms. First, we evaluated its performance in HeLa cells by transient expression (Fig. 2). Fig. 2a shows representative time-lapse images of Met-lead 1.44 M1 in the YFP and CFP channels (i and ii, respectively), along with emission ratio images (iii) obtained by dividing the fluorescence emission from the YFP channel by that from the CFP channel for each pixel, displayed as a rainbow color scale. We selected several regions of interest (ROI) within the same imaged field of view, to quantify sequential time-lapse changes in fluorescence intensities (FIs) of YFP and CFP. In the presence of Pb^{2+}, FIs for YFP increased, whereas those for CFP declined; the averaged emission ratio ranged from 2.98 ± 0.01 to 7.87 ± 0.7 (Fig. 2a, iii, and 2b; Movie S3; sensing range 264%, Table S1).

Supplementary data related to this article can be found at https://doi.org/10.1016/j.bios.2020.112571.

We also exposed HeLa cells expressing Met-lead 1.44 M1 to different concentrations of Pb^{2+} in the presence or absence of 5 μM ionomycin (this Pb^{2+} ionophore is used to artificially carry the same amounts of Pb^{2+} as in the defined buffer into living cells). The averaged time-lapse ratios (Fig. 2c and d) revealed that the detection limit (LOD) of Met-lead 1.44 M1 was at least 10 nM (152% increase, from 1.92 ± 0.001 to 2.92 ± 0.05, with ionomycin, Fig. 2c; 138% increase, from 2.07 ± 0.02 to 2.85 ± 0.05, without ionomycin, Fig. 2d; Table S3), which corresponds to a 50-fold improvement over Met-lead 1.59 (500 nM) (Chiu and Yang, 2012). The DR (at 10 μM) of Met-lead 1.44 M1 ranged from 250% (Figure 1d) to 264% (Fig. 2) up to 350% (○ in Fig. 1g), whereas that of Met-lead 1.59 ranged from 145% to 150% (3.56 ± 0.02 to 5.17 ± 0.10, □ in Fig. 1g and Fig. S11) to near 160% (Fig. 1c) (Tables S1 and S2).

3.2. Calcium channels as gates for cytosolic Pb^{2+} entry

To unveil the route of Pb^{2+} entry, we measured intracellular Pb^{2+} using Met-lead 1.44 M1 in the presence or absence of extracellular calcium ions (Ca^{2+}) in HeLa cells. Adding 50 μM or 10 μM Pb^{2+} to the culture medium resulted in significant FRET signal, as depicted in Fig. 3a and b (dashed lines): the emission ratios increased from 2.96 ± 0.02 to 7.44 ± 0.19 and 2.68 ± 0.05 to 5.68 ± 0.16, respectively. In the presence of extracellular Ca^{2+}, however, the changes in emission ratio (Δ ratio) decreased by ~3.3-fold (Fig. 3a and b, solid lines; inset bar graphs show Δ ratios). These results suggested competition between Ca^{2+} and Pb^{2+} for entry into the cytoplasm, implying that Ca^{2+} channels might be a pathway for Pb^{2+} entry.

Ca^{2+} channels are classified into two groups: voltage-gated Ca^{2+} channels (VGCCs), which play a key role in excitable cells, and store-operated Ca^{2+} channels (SOCs), the major players in Ca^{2+} signaling of non-excitable cells. As our model for further studies, we chose excitable cardiomyocytes, derived from induced pluripotent stem cells (iPSCs), as these express both VGCCs and SOCs (Wang et al., 2015; Uzun et al., 2016). Introducing 50 μM Pb^{2+} (final concentration) into the culture medium led to a Δ ratio of ~1.51 ± 0.21 (Fig. 3c–e; Movies S4–S8). By contrast, in the presence of the calcium channel inhibitors verapamil (2 μM), diltiazem (1 μM) (both VGCC blockers, Δ ratio = 0.55 ± 0.08, 0.63 ± 0.06, respectively) and 2-APB (SOC blocker, 50 μM, Δ ratio = 0.55 ± 0.12), the Δ ratio decreased 3-fold (Fig. 3d; Table S4). These results strongly suggest that Pb^{2+} can enter living cells through both VGCCs (Ferreira de Mattos et al., 2017) and SOCs (Chang et al., 2008).

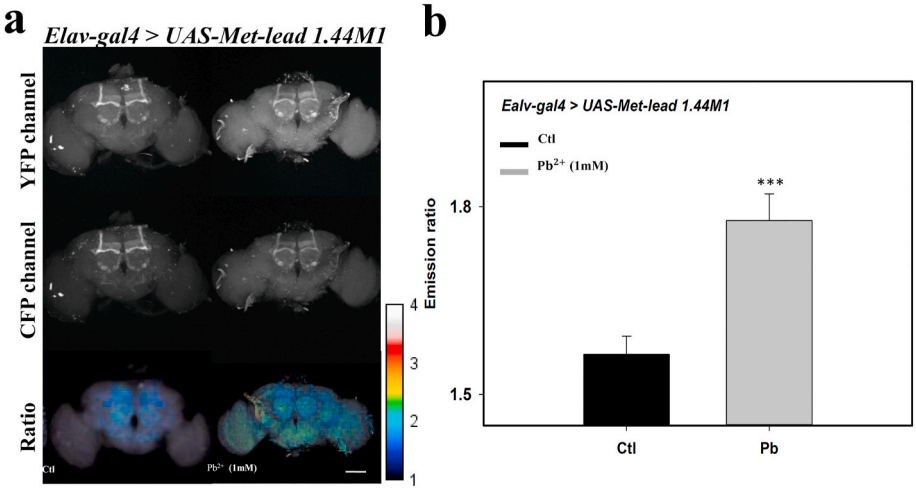

Fig. 5. *In vivo* application of Met-lead 1.44 M1. (a) Confocal FRET images of fly brains. Flies were housed without (as control) or with food containing 1 mM Pb^{2+} for 3 days. Scale bars, 100 μm. (b) Averaged emission ratios from images in (a).

Supplementary video related to this article can be found at https://doi.org/10.1016/j.bios.2020.112571

3.3. Pb^{2+} detection in plants

We also tested Met-lead 1.44 M1 in Arabidopsis to examine its performance in another Kingdom. We exposed Met-lead 1.44 M1-transfected protoplasts to 10 μM Pb^{2+} for 60 min and then performed FRET with image acquisition at time points of 0 (control), 10, 30, and 60 min (Fig. 4a, Movie S9). We calculated Δ ratios of ~2.28 (from 3.05 ± 0.03 to 5.33 ± 0.27; 175%; Table S5 and 1.35 (from 3.24 ± 0.05 to 4.59 ± 0.19; 142%; Table S6) with and without ionomycin, respectively (i, ii, Fig. 4a and b). When we exposed protoplasts to a lower concentration of Pb^{2+} (1 μM), Met-lead 1.44 M1 still detected intracellular Pb^{2+} in the presence of ionomycin, as indicated by the gradual increase of the ratio from 3.29 ± 0.05 to 4.59 ± 0.15 (ii, Fig. 4a and b; Δ ratio 1.3; 140%; Table S7).

Supplementary data related to this article can be found at https://doi.org/10.1016/j.bios.2020.112571.

Arabidopsis seedlings transiently transfected with the Met-lead 1.44 M1 construct (Zhang et al., 2006; Wu et al., 2014) were used as a testing model for FRET acquisition in intact plant tissue. We soaked seedlings in 10 μM Pb^{2+} overnight to allow time for differential distribution of lead ions and then performed FRET image acquisition. The FRET images and the emission ratios for control and Pb^{2+}-exposed seedlings of 2.18 ± 0.03 and 4.53 ± 0.04, respectively (Fig. 4c and d; Δ ratio 2.35; 208%; Table S8), clearly indicated Pb^{2+} entry and Pb^{2+} accumulation inside cotyledons in the Pb^{2+}-exposed seedlings. A detailed analysis of the magnified region of the image in Fig. 4c, ii, revealed different Δ ratios in different parts of the image (Fig. 4e, iii; from 2.68 ± 0.02, 5.25 ± 0.21 up to 10.07 ± 0.88; Δ ratios from 0.5, 3.07, up to 7.89; sensing ranges from 123%, 240%, up to 462%; Table S8), suggesting an uneven distribution of Pb^{2+} inside cotyledons. The results indicate that Arabidopsis can absorb Pb^{2+} from lead-contaminated water.

3.4. *In vivo* Pb^{2+} biosensing in fruit fly brain neurons

Finally, to test the *in vivo* biosensing ability of Met-lead 1.44 M1 in an animal model, we introduced the construct into Drosophila and used the *UAS-gal4* selection system (Jenett et al., 2012) to express the biosensor in various types of neurons within the adult fly brain. We used different promoters to drive *gal4* expression throughout all neurons of the brain (*Elav-gal4*) (Fig. 5A; Figs. S16 and S17), in cholinergic neurons (*Cha--gal4*) (Fig. S15B), and in the mushroom body (*R13F02-gal4*) (Fig. S18). Before image acquisition, we removed the skull of the fly head (Figs. S15A and S15B) to allow the emitted YFP/CFP fluorescence from neurons inside the brain to be detected.

The *in vivo* brain images of adult flies expressing Met-lead 1.44 M1 within mushroom body neurons (*R13F02-gal4* > *UAS-Met-lead 1.44 M1*) are shown in Figure S18, i and ii, for the YFP and CFP channels, and the accompanying ratio color images of the same brain region in iii and Movie S10. The derived FIs of YFP/CFP and emission ratio (Fig. S18b) revealed that the ratio values increased by 3.65-fold (365%, from 2.05 ± 0.02 to 7.48 ± 0.28; Table S9) after the introduction of 10 μM Pb^{2+} in the presence of ionomycin over the course of a 30-min recording. These significant changes clearly demonstrate an increase in intracellular Pb^{2+} inside brain neurons. When we added the metal-ion chelator, 100 μM TPEN (N,N,N′,N′-tetrakis (2-pyridinylmethyl)-1,2-ethanediamine), to the medium, the emission ratio immediately decreased back to the original value (ii, Fig. S18b), confirming that the signal changes were caused by the addition of the exogeneous Pb^{2+}.

Supplementary data related to this article can be found at https://doi.org/10.1016/j.bios.2020.112571.

To study the influence of a Pb^{2+}-contaminated environment on living organisms, we housed adult flies (*Elav-gal4* > *Met-lead 1.44 M1*) on food containing 1 mM Pb^{2+} for 3 days and then dissected their brains for imaging acquisition by confocal microscopy. In contrast to a control group of flies given normal food, lead-exposed flies showed Pb^{2+} in specific regions of the brain, as indicated by the 3D-colored FRET-ratio images (Fig. 5a). Fig. 5b depicts the deduced emission ratio from the 3D images and shows a significant increase in ratio (114%, from 1.56 ± 0.03 to 1.78 ± 0.04; Table S10). These results demonstrate that Pb^{2+} ingested from food sources can accumulate in the brain.

3.5. Optimization of met-leads, comparisons with other methods, and future perspectives

In general, the critical and limiting step in creating workable FRET-based biosensors is the selection of a suitable sensing domain that can bind the target specifically while creating enough of a structural change for detection (Miyawaki et al., 1997; Hochreiter et al., 2015). However, optimizing such tools, i.e. improving their DR (dynamic range) and LOD (sensitivity) so as to develop them into truly practical biosensing tools, requires another important and lengthy undertaking (Marx, 2017; Watabe et al., 2020).

The level of DR can be directly represented as the increased fold of FRET-ratio values (Tables S1–S10), and is largely governed by the distance change (*d*) and the anisotropy between two FRET-pair FPs that occur when the sensing target is present inside the biosensors. Taking the calcium biosensor YC 3.6 (Nagai et al., 2001, 2004) with a very high DR of nearly 600%, as a classic example, its optimization since the first-generation cameleon-1 (Miyawaki et al., 1997) (DR = 70%–150%) included a clever modification of the FPs, i.e. their circular permutation to create so-called cpFPs, and then the selection of cutting points and adoption of the linker GGSGG (Nagai et al., 2001, 2004). Another good strategy for sensor optimization is the insertion of linkers of different lengths into the sensing domain to serve as a hinge. In the case of the Met-leads series, the FRET backbone is leveraged from YC 3.6 (Miyawaki et al., 1997; Nagai et al., 2004; Chiu and Yang, 2012). The first-generation Met-lead, Met-lead 1.59 (DR = 160–170%, Chiu and Yang, 2012; and Table S2 in this study), was not fully satisfactory for the application of monitoring lead accumulation *in vivo*. We therefore continued to develop improved Met-leads by testing different lengths of sensing domains in the context of full-length PbrR. It turns out that Met-lead 1.44 (Fig. 1a), whose sensing area contains an additional α-helix from PbrR 1.44 (Fig. S4, middle), has a better DR than Met-lead 1.59 (200% in Met-lead 1.44 vs. 150% in Met-lead 1.59; Fig. 1c). Using Met-lead 1.44 as a starting point, we further inserted a repeat sequence (linker) in the middle position of PbrR to form Met-lead 1.44 M1, which displays a relatively low basal ratio level compared to Met-lead 1.44 (2.37 ± 0.01 in Met-lead 1.44 M1 vs. 3.25 ± 0.06 in Met-lead 1.44; Fig. 1b). We observed that the DR of Met-lead 1.44 M1 ranged from 250% to 460% (both in living single human cells, in Arabidopsis seedlings and Drosophila brain tissue *in vivo*; Tables S1, S8 and S9), which is the highest among all versions of Met-lead sensors developed thus far (Fig. 1d, g, 2b, 2c and 4e; Fig. S18).

In terms of the LOD, a valuable index to define the sensing capability of biosensors is their individual K_d, which can be calculated through titration experiments (Fig. 1g). The original K_d of intact PbrR (with its DNA BD) was reported to be 198 ± 16 nM (in bacteria) (Chen et al., 2005), a bit higher than the BLL safety levels in children (3 μg/dL, 150 nM), but similar to the K_d of the Met-lead 1.59 (66 nM, calculated from in-cell data in this study; or 69 nM, from a previous report that characterized purified Met-lead proteins (Chiu and Yang, 2012)). However, the practical sensing limit of Met-lead 1.59 is in reality 500 nM (Chiu and Yang, 2012). After further optimization of the length of the sensing domain, and upon addition of the linker, the improved version of Met-lead 1.44 M1 has a K_d of 25.97 nM (Fig. 1g) and a practical sensitivity of 10 nM (Fig. 2c and d; Table S3), which is five times below the WHO-permitted level of Pb^{2+} in tap water of 10 ppb (WHO, 2017), and fifteen times lower than the BLL for children, 3 μg/dL. These noteworthy improvements in the Met-lead DR and LOD appear to be due to the

Table 1
Comparison of characteristics of different methods for Pb^{2+} sensing.

Methods	Limit of detection (sensitivity)	Specificity (ion selectivity)	Assay format	Advantages (+)/disadvantages (−)	Cost-efficiency	Ref.
Graphene oxide (GO)-based DNAzyme	0.3 nM (calculated) 10–20 nM	Hg^{2+}, Zn^{2+}, Co^{2+}, Cd^{2+}, Mn^{2+}, Ca^{2+}, Ni^{2+}, Cu^{2+}, Fe^{3+}	*in vitro* (river water)	20 min (+)/in-cell not practically tested (−)	High	1
Graphene quantum dots (GQDs)-aptamer (G-quadruplex) probe	0.6 nM (calculated) 50–100 nM	Ag^{+}, Fe^{2+}, Ca^{2+}, Co^{2+}, Cu^{2+}, Hg^{2+}, Cd^{2+}, Ni^{2+}, K^{+}, Mg^{2+}, Zn^{2+}, Ba^{2+}, Fe^{3+}	*in vitro;* *in vivo* (expected from biocompatibility)	Fast (1 min), photobleaching resistance (+)/not practically tested (−)	High	2
Metal-peptide supramolecular assembly (GSSH-2TPE)	1.5 nM (calculated) 100 nM	Ni^{2+}, Hg^{2+}, Li^{+}, Mg^{2+}, Cu^{2+}, Co^{2+}, Ca^{2+}, Cr^{3+}, K^{+}, Na^{+}, Fe^{3+}, Al^{3+}, Ag^{+}, Ba^{2+}, Cd^{2+}, Zn^{2+}, Mn^{2+}, Fe^{2+}	In-cell; *in vitro*	Good cell permeability, non-toxic (+)/Al^{3+} (−)	Medium	3
Near-infrared fluorescent probe (NIR-PbP)	–	Zn^{2+}, Fe^{2+}, Hg^{2+}, Cd^{2+}, Ca^{2+}, Co^{2+}, Cu^{2+}, Mg^{2+}, Ni^{2+}, Na^{+}, K^{+}	In-cell; *in vitro* (environment)	*In vivo* possible; color change (+)/LOD unknown (−)	Medium	4
FRET-based Met-lead 1.59	500 nM (experimental data)	Ca^{2+}, Mg^{2+}, Mn^{2+}, Fe^{2+}, Cu^{2+}, Zn^{2+}	In-cell	Fast (+)/poor LOD; need transfection (−)	Medium	5
FRET-based Met-lead 1.44 M1	10 nM (experimental data)	Ca^{2+}, Mg^{2+}, Mn^{2+}, Fe^{2+}, Co^{2+}, Cu^{2+}, Zn^{2+}	In-cell; *in vivo*; environment (*in vitro*)	Combine *in vivo* and *in vitro*; fast (+)/need transfection (−)	Medium	6, 7

- indicates values not reported.
Ref: 1. Zhao et al. (2011); 2. Qian et al. (2015); 3. Gui et al. (2019); 4. Bi et al. (2017); 5. Chiu and Yang (2012); 6. Yang et al. (2020); 7. This study.

additional α-helix and linker. A general comparison of the methods for Pb^{2+} sensing, e.g. graphene oxide-based DNAzyme, quantum dots (QDs), metal-peptide supramolecular assembly, near-infrared fluorescent probes, and the FRET-based method, is shown in Table 1. To the best of our knowledge, most of the lead detection methods (*in vitro*/in-cell/*in vivo*) were designed for inorganic Pb^{2+} (He et al., 2006; Zhao et al., 2011; Chiu and Yang, 2012; Qian et al., 2015; Bi et al., 2017; Yang et al., 2017; Zhang et al., 2017; Gui et al., 2019; Yang et al., 2020; this manuscript; also, Table 1). In the future, we expect that novel lead biosensor(s) can be developed to tackle organic lead sources.

In regards to the possible clinical applications of Met-lead 1.44 M1, it will be important to distinguish free Pb^{2+} in body fluids (e.g. blood plasma; Fig. S19a; ratio value from control 3.58 ± 0.05 up to 6.30 ± 0.40 at 10 μM and 8.58 ± 0.65 at 100 μM) and cellular uptake of Pb^{2+} (e.g. the blood cells; Fig. S19b; ratio value from control 1.23 ± 0.02 up to 1.64 ± 0.07 at 10 μM), from which a new definition of BLL can be provided. To this aim, the separated blood plasma from blood samples will be put onto a chip where purified Met-lead 1.44 M1 can be immobilized (method under development; so far, we used Met-lead 1.44 M1-expressing HeLa cells as a sensing tool for serum as shown in Fig. S19a) for the measurement of the Pb^{2+} concentration with the same FRET platform. In parallel, blood cells can be isolated from whole blood, transduced with Met-lead 1.44 M1 through a general virus approach as described in this study, and examined under the FRET imaging platform also demonstrated in this study.

4. Conclusions

In summary, we have developed an improved FRET-based heavy metal biosensor, Met-lead 1.44 M1, with high performance. The LOD (sensitivity) of Met-lead 1.44 M1 is 10 nM, equivalent to 0.2 μg/dL (or 2.0 ppb), 15 times lower than the official safe BLL for children of 3 μg/dL (and five times below the WHO-permitted level of lead in tap water of 10 ppb). Therefore, it has great potential for use in both low BLL measurements and the rapid detection of environmental lead contamination at very low concentrations. The DR of Met-lead 1.44 M1 in FRET-ratio ranges was as high as ~5-fold (in cotyledons of Arabidopsis seedlings). Its creation confirms the feasibility of developing an *in vivo* lead detection biosensor. The Pb^{2+} sensing ability of Met-lead 1.44 M1 has been demonstrated in both single-cell and whole-body (*ex vivo* and *in vivo*) contexts. Thus, this sensor provides a powerful tool both for advanced research into the effects of low BLLs and environmental lead contamination and for practical applications such as fast environmental Pb^{2+} detection and other studies of lead poisoning.

Author contributions

D.M.Y., Y.F.C. and T.Y.C. designed the variants of the Met-lead biosensors and the experiments. T.Y.C. performed cloning, some of the live-cell lead biosensing, lead titration, and analysis to determine the dissociation constants (K_ds) of the Met-leads. C.S.L. provided the protoplasts, designed the Agrobacterium method for transformation of Arabidopsis seedlings, and generated transgenic Arabidopsis plants. H.Y.H. assisted with project design and performed most of the *in vitro* and plant- and Drosophila-related FRET imaging. T.F.F. provided the fly strains and created the UAS strains, including *UAS-Met-lead 1.59* and *UAS-Met-lead 1.44 M1*. Y.S.L. and H.Y.H. performed some of the *in vivo* and *ex vivo* fly brain lead biosensing experiments. Y.S.L. and M.W.C. performed the 3D molecular simulation of Met-leads. D.M.Y. wrote the manuscript, and Y.F.C., M.W.C., and R.V.M. co-wrote the manuscript.

CRediT authorship contribution statement

De-Ming Yang: Conceptualization, Methodology, Investigation, Writing - original draft, Project administration, Supervision, Validation, Writing - review & editing. **Tsai-Feng Fu:** Investigation. **Choun-Sea Lin:** Investigation. **Tai-Yu Chiu:** Conceptualization, Methodology, Data curation, Formal analysis, Visualization, Funding acquisition. **Chien-Chang Huang:** Data curation, Formal analysis, Visualization, Funding acquisition. **Hsin-Yi Huang:** Data curation, Formal analysis, Visualization, Funding acquisition. **Min-Wen Chung:** Investigation. **Yu-Syuan Lin:** Data curation, Formal analysis, Visualization, Funding acquisition. **Robeth Viktoria Manurung:** Investigation. **Yu-Fen Chang:** Conceptualization, Methodology, Investigation, Project administration, Supervision, Validation, Writing - review & editing.

Declaration of competing interest

The authors declare that they have no known competing financial interests or personal relationships that could have appeared to influence the work reported in this paper.

Acknowledgements

This work was financially supported by MOST (105-2320-B-075-002, 108-2745-8-075-001-) and Taipei Veterans General Hospital (V106C-194, V107C-008). We thank the "Translational biomedical imaging platform of the National Core Facility for Biopharmaceuticals, Ministry of Science and Technology, Taiwan" for technical support with image acquisition and analysis. We are grateful to NEXEL, Ltd. For the iPSC-cardiomyocytes and detailed culture instructions.

Appendix A. Supplementary data

Supplementary data to this article can be found online at https://doi.org/10.1016/j.bios.2020.112571.

References

Azad, T., Tashakor, A., Hosseinkhani, S., 2014. Split-luciferase complementary assay: Applications, recent developments, and future perspectives. Anal. Bioanal. Chem. 406, 5541–5560.

Bischof, H., et al., 2019. Live-cell imaging of physiologically relevant metal ions using genetically encoded FRET-based probes. Cells 8, 492.

Bi, J.H., et al., 2017. Near-infrared fluorescent probe for sensitive detection of Pb(II) ions in living cells. Inorg. Chim. Acta. 468, 140–145.

Borremans, B., Hobman, J.L., Provoost, A., Brown, N.L., van Der Lelie, D., 2001. Cloning and functional analysis of the pbr lead resistance determinant of *Ralstonia metallidurans* CH34. J. Bacteriol. 183, 5651–5658.

Caldwell, K.L., et al., 2017. Measurement challenges at low blood lead levels. Pediatrics 140, e20170272.

Caldwell, K.L., et al., 2019. LAMP: A CDC program to ensure the quality of blood-lead laboratory measurements. J. Publ. Health Manag. Pract. 25. Suppl. 1, Lead Poisoning Prevention: S23-S30.

Carter, K.P., Young, A.M., Palmer, A.E., 2014. Fluorescent sensors for measuring metal ions in living systems. Chem. Rev. 114, 4564–4601.

Chang, Y.F., et al., 2008. Orai1-STIM1 formed store-operated Ca^{2+} channels (SOCs) as the molecular components needed for Pb^{2+} entry in living cells. Toxicol. Appl. Pharmacol. 227, 430–439.

Changela, A., et al., 2003. Molecular basis of metal-ion selectivity and zeptomolar sensitivity by CueR. Science 301, 1383–1387.

Chen, C.C., Hwang, J.K., Yang, J.M., 2006. $(PS)^2$: Protein structure prediction server. Nucleic Acids Res. 34, W152–W157 (Web Server issue).

Chen, P., et al., 2005. An exceptionally selective lead(II)-regulatory protein from *Ralstonia metallidurans*: Development of a fluorescent lead(II) probe. Angew. Chem. Int. Ed. 44, 2715–2719.

Chiu, T.Y., Yang, D.M., 2012. Intracellular Pb^{2+} content monitoring using a protein-based Pb^{2+} indicator. Toxicol. Sci. 126, 436–445.

Chiu, T.Y., Chen, P.H., Chang, C.L., Yang, D.M., 2013. Live-cell dynamic sensing of Cd^{2+} with a FRET-based indicator. PloS One 8 e65853.

Ferreira de Mattos, G., Costa, C., Savio, F., Alonso, M., Nicolson, G.L., 2017. Lead poisoning: acute exposure of the heart to lead ions promotes changes in cardiac function and Cav 1.2 ion channels. Biophys Rev 5, 807–825.

Flora, G., Gupta, D., Tiwari, A., 2012. Toxicity of lead: A review with recent updates. Interdiscipl. Toxicol. 5, 47–58.

Frank, J.J., Poulakos, A.G., Tornero-Velez, R., Xue, J., 2019. Systematic review and meta-analyses of lead (Pb) concentrations in environmental media (soil, dust, water, food, and air) reported in the United States from 1996 to 2016. Sci. Total Environ. 694, 133489.

Gui, S., Huang, Y., Zhu, Y., Jin, Y., Zhao, R., 2019. Biomimetic sensing system for tracing Pb^{2+} distribution in living cells based on the metal-peptide supramolecular assembly. ACS Appl. Mater. Interfaces 11, 5804–5811.

He, Q., Miller, E.W., Wong, A.P., Chang, C.J., 2006. A selective fluorescent sensor for detecting lead in living cells. J. Am. Chem. Soc. 128, 9316–9317.

Hochreiter, B., Pardo-Garcia, A., Schmid, J.A., 2015. Fluorescent proteins as genetically encoded FRET biosensors in life sciences. Sensors 15, 26281–26314.

Hosseini, E.S., et al., 2020. The Lumiptosome, an engineered luminescent form of the apoptosome can report cell death by using the same Apaf-1 dependent pathway. J. Cell Sci. 133, jcs242636.

Hu, A., Zhang, W., Wang, Z., 2010. Functional feedback from mushroom bodies to antennal lobes in the *Drosophila* olfactory pathway. Proc. Natl. Acad. Sci. U. S. A. 107, 10262–10267.

Huang, T.T., et al., 2015. $(PS)^2$: Protein structure prediction server version 3.0. Nucleic Acids Res. 43 (W1), W338–W342.

Jenett, A., et al., 2012. A GAL4-driver line resource for *Drosophila* neurobiology. Cell Rep. 2, 991–1001.

Lanphear, B.P., Rauch, S., Auinger, P., Allen, R.W., Hornung, R.W., 2018. Low-level lead exposure and mortality in US adults: A population-based cohort study. Lancet Public Health 3, 177–184.

Marx, V., 2017. Probes: FRET sensor design and optimization. Nat. Methods 14, 949–953.

Miyawaki, A., et al., 1997. Fluorescent indicators for Ca^{2+} based on green fluorescent proteins and calmodulin. Nature 388, 882–887.

08 Molecular Operating Environment (MOE), 2013. Chemical Computing Group Inc., 1010 Sherbooke St. West, Suite #910, Montreal, QC, Canada, H3A 2R7, 2017.

Nagai, T., Sawano, A., Park, E.S., Miyawaki, A., 2001. Circularly permuted green fluorescent proteins engineered to sense Ca^{2+}. Proc. Natl. Acad. Sci. U.S.A. 98, 3197–3202.

Nagai, T., Yamada, S., Tominaga, T., Ichikawa, M., Miyawaki, A., 2004. Expanded dynamic range of fluorescent indicators for Ca^{2+} by circularly permuted yellow fluorescent proteins. Proc. Natl. Acad. Sci. U.S.A. 101, 10554–10559.

Needleman, H., 2004. Lead poisoning. Annu. Rev. Med. 55, 209–222.

O'Connor, D., Hou, D., Ok, Y.S., Lanphear, B.P., 2020. The effects of iniquitous lead exposure on health. Nat Sustain 3, 77–79.

Patterson, C.C., 1956. Age of meteorites and the earth. Geochem. Cosmochim. Acta 10, 230–237. https://doi.org/10.1016/0016-7037(56)90036-9.

Patterson, C.C., 1965. Contaminated and natural lead environments of man. Arch. Environ. Health 11, 344–360. https://doi.org/10.1080/00039896.1965.10664229.

Paulson, J.A., Brown, M.J., 2019. The CDC blood lead reference value for children: time for a change. Environ. Health 18, 16.

Qian, Z.S., Shan, X.Y., Chai, L.J., Chen, J.R., Feng, H., 2015. A fluorescent nanosensor based on graphene quantum dots–aptamer probe and graphene oxide platform for detection of lead (II) ion. Biosens. Bioelectron. 68, 225–231.

Reuben, A., et al., 2017. Association of childhood blood-lead levels with cognitive function and socioeconomic status at age 38 years and with IQ change and socioeconomic mobility between childhood and adulthood. J. Am. Med. Assoc. 317, 1244–1251.

Rocha, A., Trujillo, K., 2019. Neurotoxicity of low-level lead exposure: history, mechanisms of action, and behavioral effects in humans and preclinical models. Neurotox 73, 58–80.

Sameach, H., et al., 2017. Structural and dynamics characterization of the MerR family metalloregulator CueR in its repression and activation states. Structure 25, 988–996.

Uzun, A.U., et al., 2016. Ca(2+)-currents in human induced pluripotent stem cell-derived cardiomyocytes effects of two different culture conditions. Front. Pharmacol. 7, 300.

Wang, Y., et al., 2015. Nitric oxide-cGMP-PKG pathway acts on orai 1 to inhibit the hypertrophy of human embryonic stem cell-derived cardiomyocytes. Stem cells 33, 2973–2984.

Watabe, T., Terai, K., Sumiyama, K., Matsuda, M., 2020. Booster, a red-shifted genetically encoded Förster resonance energy transfer (FRET) biosensor compatible with cyan fluorescent protein/yellow fluorescent protein-based FRET biosensors and blue light-responsive optogenetic tools. ACS Sens. 5, 719–730.

World Health Organization, 2017. Guidelines for Drinking-Water Quality. + 1s t add, 4 th ed. WHO, Geneva. accessed 26 May 2020. https://apps.who.int/iris/handle/10665/254637.

Wu, H.Y., et al., 2014. AGROBEST: An efficient *Agrobacterium*-mediated transient expression method for versatile gene function analyses in *Arabidopsis* seedlings. Plant Methods 10, 19.

Wu, F.H., et al., 2009. Tape-*Arabidopsis* Sandwich - a simpler *Arabidopsis* protoplast isolation method. Plant Methods 5, 16.

Yang, D., et al., 2017. Aptamer-based biosensors for detection of lead(II) ion: a review. Anal. Methods 9, 1976–1990.

Yang, D.M., et al., 2020. Monitoring the heavy metal lead inside living *Drosophila* with a FRET-based biosensor. Sensors 20, 1712.

Zhao, X.H., et al., 2011. Graphene–DNAzyme based biosensor for amplified fluorescence "turn-on" detection of Pb^{2+} with a high selectivity. Anal. Chem. 83, 5062–5066.

Zhang, D., et al., 2017. Ratiometric fluorescent detection of Pb^{2+} by FRET-based phthalocyanine-porphyrin dyads. Inorg. Chem. 56, 14533–14539.

Zhang, X., Henriques, R., Lin, S.S., Niu, Q.W., Chua, N.H., 2006. *Agrobacterium*-mediated transformation of *Arabidopsis thaliana* using the floral dip method. Nat. Protoc. 1, 641–646.